https://doi.org/10.48048/tis.2022.6326

Experimental Investigation of Heat and Fluid Flow Characteristics on Expanded Metal Mesh Roughened Solar Collector

Yewondwosen Gzate Ayalew

Department of Mechanical Engineering, Gondar Institute of Technology, University of Gondar, Gondar, Ethiopia

(Corresponding author's e-mail: ygzate@gmail.com, yewondwosen.gzate@uog.edu.et)

Received: 27 August 2021, Revised: 4 October 2021, Accepted: 27 October 2021, Published: 2 November 2022

Abstract

Solar air heater is used for agricultural grain products drier, curing of industrial products and for other systems requiring low grade thermal energy. Their usefulness and quantitative energy collections has been limited. This is because of low thermal efficiency with primarily as a result of low convective heat transfer coefficient, between the absorber plate and air leading to higher plate temperature. This results greater thermal energy losses. Experimental investigation has been conducted to study heat transfer enhancement by using small diameter wire ribs on absorber plate of solar air heater duct, with the roughened wall exposed to the glazing side while the remaining 3 walls were insulated. The roughened wall has relative roughness height (e/D_h) 0.0135 - 0.0406, relative roughness pitch (p/e) 10 - 20, rib height 0.5 - 1.5 mm, expanded metal mesh (L/e) 25 - 75, Short way mesh (S/e) 15 - 45, angle of attack 45° for inclined configuration, duct aspect ratio of 12 and the air flow rate corresponds to Reynolds number between 2,000 to 18,000. It has been found that the heat transfer coefficient could be improved by a factor up to 2.2 and the friction factor had been found to increase by a factor of 1.2 times that of the smooth duct. The investigation emphasized that the secondary flow rolling along the inclined ribs is responsible for higher heat transfer rates. Thermal efficiency increased from 50.58 - 65.75 %. Finally, correlation is developed for both Nusselt number and friction factor using sigma plot software, which can be selected by the designer for a given operating condition.

Keywords: Solar air heater, Wire rib roughness, Air duct, Expanded metal mesh, Dryer

Introduction

Now a days, there is a growing awareness that renewable energy has an important role to play in extending technology to the farmers in developing countries to increase their productivity. Solar energy is one of efficient and effective with freely available renewable energy [1]. Solar thermal technology is rapidly gaining acceptance as an energy saving measure in agricultural applications [1,2]. To make effective and efficient, solar thermal technology, different researchers are dealing highly to increase its, efficiency. Still its improvement and finding new technology is in progress [3]. Solar energy is captured by solar collector. Solar air heaters are non-concentric type of solar collector which are made up of black coated surface to absorb maximum sun ray. Flat plate solar air heaters, heat air by utilizing solar energy and it is used in many applications requiring low to moderate temperature with below 100 °C, such as crop drying and space heating, curing of industrial products etc. [4,5]. The components of a solar air heater includes an absorber plate, air flow channel, insulation for the bottom and lateral sides of the solar collector and cover glass [6].

Food scientists, mostly suggested that by reducing the moisture content of food grains between 10 - 20 %, bacteria, yeast, mold and enzymes for all intents and purposes are prevented from spoiling of the grain, actually contrary to popular belief [7]. Solar air heaters are used for agricultural products grain dryer, seasoning of timber, curing of industrial products and for systems requiring low grade thermal energy. Even if it has many applications, its usability is limited. This is because of low existence of heat transfer coefficient between the absorber plate and flowing fluid [8-10]. The cause of obtaining low heat transfer coefficient is formation of laminar sub layer between flat plate solar absorber and flowing fluid.

Different techniques mostly are really suggested and applied for the most part improve the heat transfer coefficient between the absorber plate and air. Among them one for the most part is installation of turbulence promoters in the form of sort of artificial roughness on the underside of the absorber plate, which

is significant. Such particularly artificial roughness produces turbulence and breaks the laminar sub layer definitely due to this much more heat transfer definitely is achieved [11].The objective of this work actually is to conduct experimental investigation on fluid flow and heat transfer characteristics on kind of upper broad wall definitely circular wire rib as artificial roughness using rectangular duct.

(a) Curing of industrial products (b) Agricultural grain product dryer (c) Seasoning of timber

Figure 1 Applications of solar air heaters [12-14].

Materials and methods

The input data for the most part has been taken on basis of really practical considerations of system and operating conditions which kind of are taken from the literature, which definitely is quite significant [15-18]. These parameters for the most part include basically relative roughness pitch (P/e) distance between consecutive ribs per roughness height (e/D_h), particularly relative roughness height (e/D_h) roughness height per hydraulic diameter of duct, basically short way mesh (S/e), kind of long way mesh (L/e) and Reynolds number (Re).

Table 1 Range of parameters (input data).

Parameters	Range
Relative roughness height (e/D)	0.0135 - 0.0406
Relative roughness pitch (p/e)	10 - 20
Long side per roughness height (L/e)	25 - 75
Short side per roughness height (S/e)	15 - 45
Reynold number (Re)	2,000 - 18,000

Solar air heater duct model

Figures 2 and **3** below are taken for analysis.

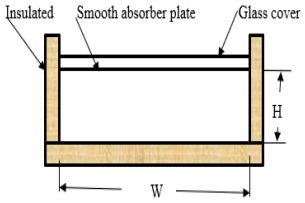

Figure 2 Four sides are smooth duct.

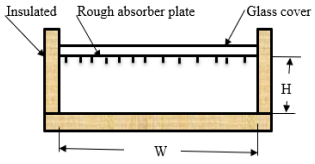

Figure 3 One side rough and others are smooth duct.

Fluid flow analysis

The analysis follows the approach [19] who studied on the fluid flow in three side roughened and 1 side basically smooth duct and [20], who studied about computational investigation on thermal performance of solar air heater having roughness elements as really transverse wire on the 2-side absorber plat. The above 2 ducts actually have similar cross-section area of (W×H) with W >> H [20], demonstrating that the above 2 ducts kind of have similar cross-section area of (W×H) with W >> H [20], which definitely is significant. In case of fully developed turbulent flow in a 4-sided very smooth duct, the friction factor really is written as follows [21], or so they essentially thought.

$$f_s = \frac{\tau_s}{\frac{1}{2}\rho {v_s}^2} \quad (1)\ [21]$$

Where f_s = friction factor in the smooth.
τ_s = shear stress in the smooth.
ρ = density of air.
v_s = velocity of air in the smooth.

In similar methodology the friction factor in a 4-sided rough duct is expressed as follows [22]:

$$f_r = \frac{\tau_r}{\frac{1}{2}\rho {v_r}^2} \quad (2)\ [22]$$

Where f_r = friction factor in the rough surface.
τ_r = shear stress in the rough duct.
v_r = velocity of air in the rough duct.

Again actually average friction factor for fully developed turbulent flow for a 4-sided duct with 3 sides particularly are smooth is written as in a definitely big way [23]:

$$f_{av} = \frac{\tau_{av}}{\frac{1}{2}\rho v^2} \quad (3)\ [24]$$

The shear forces of the duct system are written as follows:

$$[(2W + 2H)\,\tau_{av}]L = [(W + 2H)\,\tau_{3s} + W\tau_r]L \quad (4)\ [25]$$

$$\overline{f_r} = \frac{(W)\left[\frac{2}{\left[0.95\left(\frac{p}{e}\right)^{0.53} + 2.5\ln\left(\frac{D_h}{2e}\right) - 3.75\right]^2}\right] + (W+2H)f_s}{2(W+H)} \quad (5)\ [26,27]$$

Heat transfer analysis

According to [30,31] the equation of Webb *et al*. 1971 can be used for similar roughness geometry which is given by:

$$St_r = \frac{f_r/2}{1 + \sqrt{\left(\frac{f_r}{2}\right)}\left[4.5\,(e^+)^{0.29}\,pr^{0.57} - 0.95\left(\frac{p}{e}\right)^{0.53}\right]} \quad (6)\ [30,31]$$

Eq. (6) above is for 4-sided rough rectangular duct and it is again for tube, but in this case the 1 side rough and 3 side smooth. So, the average value of $\overline{f_r}$ and average value of $\overline{St_r}$ are used in place of f_r and St_r and the equation becomes:

$$\overline{Nu_r} = \frac{\overline{f_r}/2}{1 + \sqrt{\left(\frac{f_r}{2}\right)}\left[4.5\,(e^+)^{0.29}\,pr^{0.57} - 0.95\left(\frac{p}{e}\right)^{0.53}\right]} R_e\, P_r \quad (7)\ [31]$$

Experimental set up arrangement

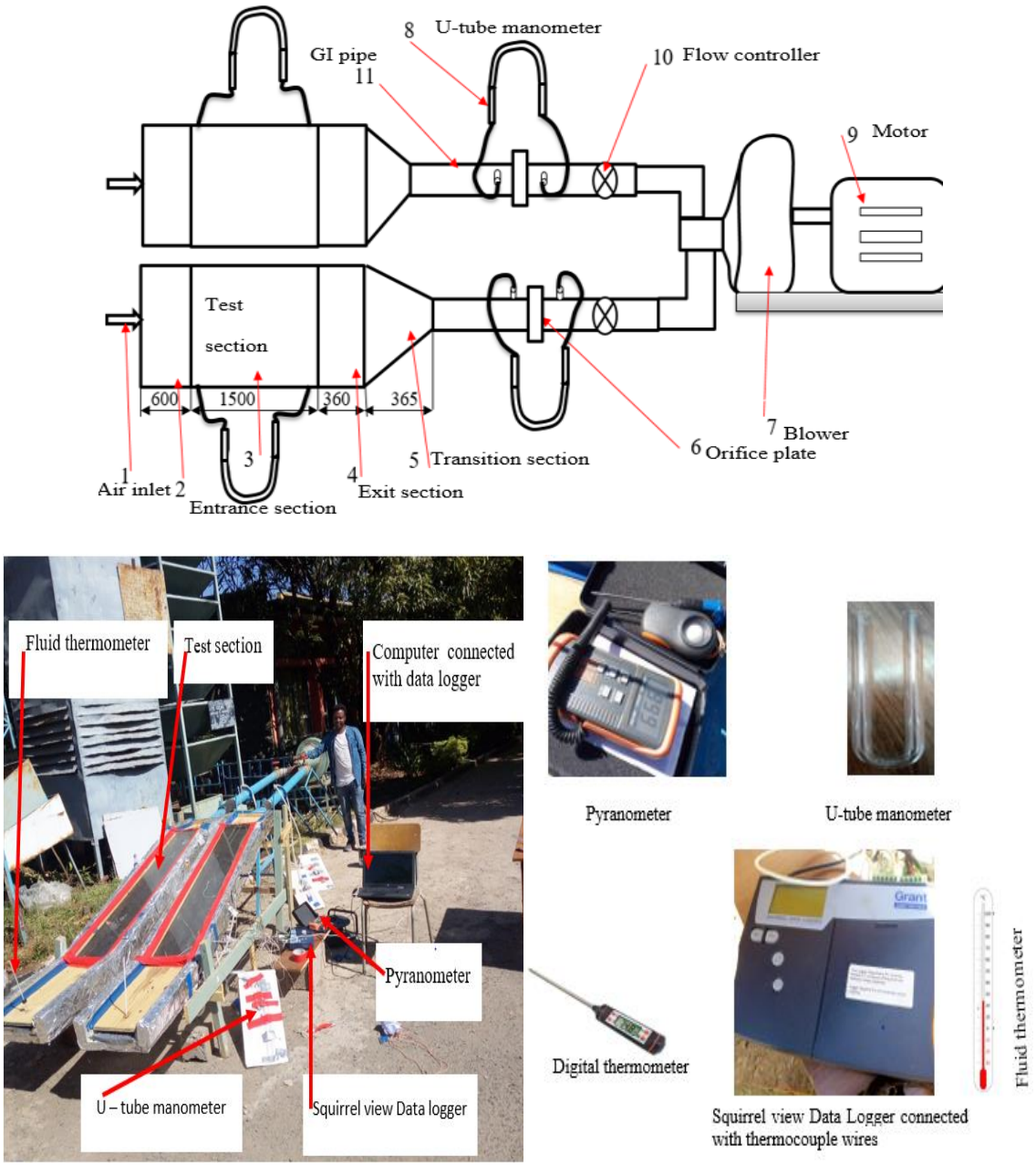

Figure 4 Schematic diagram and photographic view of experimental set up with instruments.

Absorber plate metal mesh

Overall dimension of the absorber plate is given by 1500×240×1.5 mm^3 length, width and thickness, respectively.

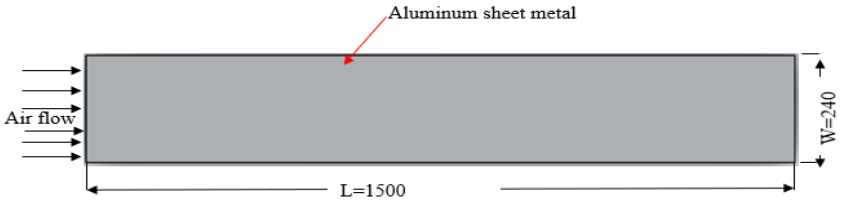

(a) Smooth plate

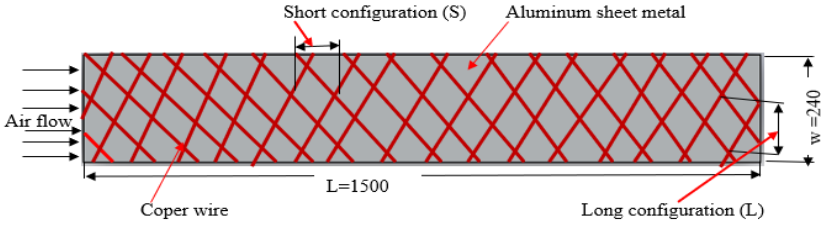

(b) Rough plate (copper wire twisted on aluminum sheet)

Figure 5 Solar absorber plate drawn by solid work (all dimensions are in mm).

Energy balance on the solar collector

Energy balance on the absorber plate is calculated by equating the fairly total heat mostly gained by definitely soar radiation on the absorber plate to the really total heat loss from the absorber plate, which particularly quite significant [33].

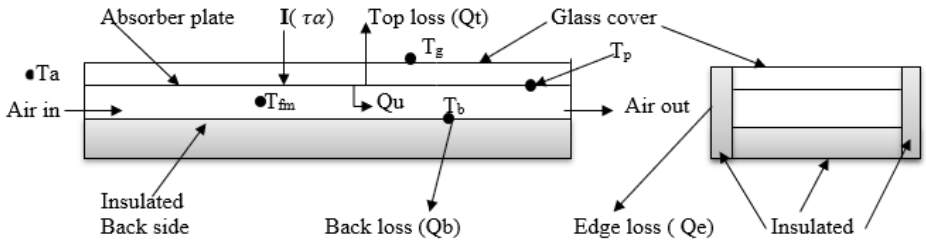

Figure 6 Energy balance on the solar collector.

From **Figure 6** conservation of energy, heat gain = heat loss. Then the following thermal energy equation is developed [36].

$$I \times A_c \times \tau = Q_{useful} + Q_{cond} + Q_{conve} + Q_{radition} + Q_{\rho} \quad (8)\ [33]$$

Where I = Rate of total radiation incident on the absorber's surface.

Ac = collector area.

Qu = rate of useful energy collected by the air.

Q_{cond} = rate of conduction losses from the absorber.

Qconv = rate of convective losses from the absorber.

Q_{rad} = rate of long wave radiation from the absorber.

Qρ = rate of reflection losses from the absorber.

τ = is transmittivity of the glass.

Instrumentation

The instrumentation process specifically covers measuring of pressure, solar radiation and air and pate temperature [34].

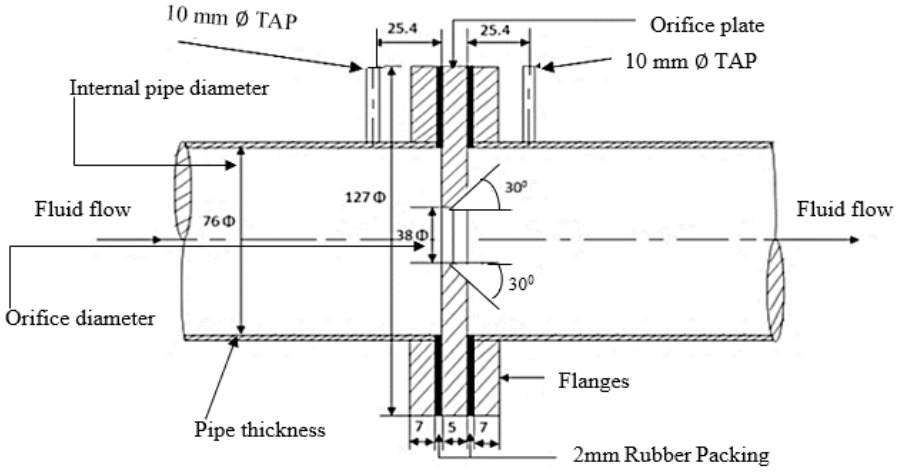

Figure 7 Orifice TAP location and detail view of orifice meter assembly.

Temperature measurement

Temperature of the plate is measure by contact thermocouple. Eight number of points are taken from the absorber plate face and measured the temperature value. The numbers of points are taken as to cover the average plate temperature.

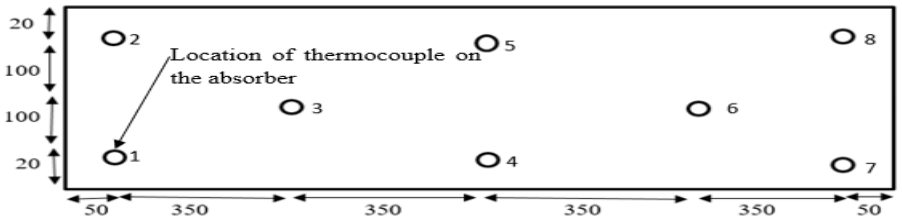

Figure 8 Location of thermocouples on absorber plat (all dimensions are in mm).

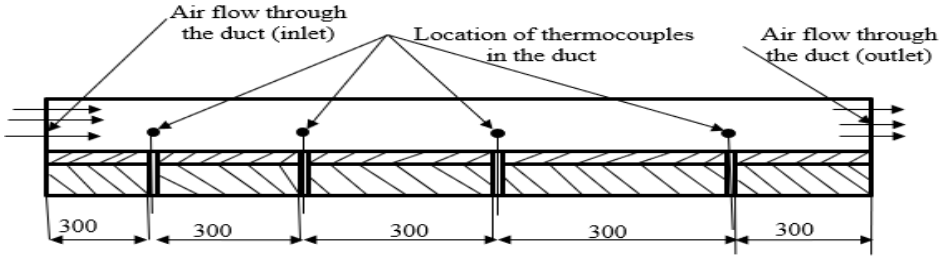

Figure 9 Location of thermocouples and air taps inside the duct (all dimensions are in mm).

Table 2 List of measuring instruments and their accuracy level.

No.	Type of measuring Instruments	Error (%)
1	Glass thermometer	±1.11
2	Digital thermometer	±2.67
3	Pyranometer (solar power meter)	±3.538
4	U-tube manometer	±1.12

Experimental testing procedure

The experimental test procedure definitely starts first by checking to generally make kind of sure that all measuring instruments are particularly functional and installed correctly, which mostly is quite significant. Then the following parameters are measured.

1) Pressure drops (ΔP) across the orifice plate for both ducts.
2) Pressure drops (ΔP) across test section for both ducts.
3) Temperature of the absorber plate both smooth and rough.
4) Fluid temperature inside the duct.
5) Intensity of solar radiation.

Data reduction

The data reduction includes literally to calculate the following parameters in a sort of major way. Therefore, all intents and purposes whole analysis follows the same procedure, which is fairly significant. For example, for generally smooth plate definitely run numbe1 (10:00 A.M) the analysis actually is done as follows.

1) Average plate temperature: This for the most part is done by summing all measured value of plate temperature divided by the number of points taken as measured value [35]:

$$\overline{T_P} = \frac{Tp_1 + Tp_2 + Tp_3 + \ldots + Tp_n}{n} \quad (9)\ [35]$$

2) Average air temperature: This is calculated by [36]:

$$\overline{T_f} = \frac{Tf_1 + Tf_2 + Tf_3 + \ldots + Tf_n}{n} \quad (10)\ [36]$$

3) Pressure difference: The change in pressure difference mostly is calculated by using the following formulas [37]:

$$P_1 - P_2 = g \times \Delta h \times \rho_f \left(\frac{\rho_m}{\rho_f} - 1\right) \quad (11)\ [37]$$

Where P_1= upstream pressure (pressure before orifice inlet).
P_2 = downstream pressure (pressure after orifice meter outlet).
h = differential at restriction, liquid column height.
ρ_m = density of manometric fluid.
ρ_f = density of measured fluid.
g = acceleration due to gravity.

1) Mass flow rate: To calculate the mass flow rate of the following fluid, first the throat velocity and Reynolds number should kind of be specifically known. These are given by [38]:

$$V_{throat} = \left[\frac{2\,\Delta p}{\rho\,(1 - \beta^4)}\right]^{0.5} \quad (11)\ [38]$$

The mass flow rate is calculated using the equation [39]:

$$\dot{m} = C_d \times A_O \times \left[\frac{2 \times \rho f \times \Delta porifice}{1 - \beta^4}\right]^{0.5} \quad (12)\ [39]$$

Where $\dot{m}$ = mass flow rate.
Cd = descharging coefficient.
Ao = area of orifice meter.
ρ_f = density of air.
β = The ratio of diameter of orfice to the internal diameter of the pipe.
ΔP = presure difernce.

2) Velocity of air: It is calculated as follows:

$$V = \frac{\dot{m}}{A \times \rho} \quad (13)\ [40]$$

Where $\dot{m}$ = mass flow rate of air.
A = area of duct.
V = velocity of air.
ρ = density of air.

3) Reynold number: It is dimensionless parameter which is the ration of inertia force to viscous force and it depends up on the velocity of the fluid, the hydraulic diameter of the duct, density of air and viscosity of the fluid in this case air are related as follows:

$$Re = \frac{V \times D_h}{\nu} \quad (14)$$

Where Re = Reynold number.
V = velocity of air in the duct.
D_h = hydraulic diameter of the rectangular duct.
ν = kinematic viscosity of air at mean fluid temperature.

4) Heat gain by the air: The use full amount of heat gain by the air. It is calculated as follows [42]:

$$Q_u = \dot{m} \times C_p \times (Tf_o - Tf_i) \quad (15)\ [41]$$

Where Qu = heat gain by the air.
C_p = specific heat of air.
Tf_o = outlet air temperature.
Tf_i = inlet air temperature.

5) Convective heat transfer coefficient: The convective heat transfer coefficient is determined by relating heat gain by air equivalent with heat loss from the plate [42]. Which is use full heat gain by air = heat loss from the plate by the flowing fluid (air).

$$\dot{m} \times C_p \times (T_o - T_i) = h \times A_p \times (\overline{T_P} - \overline{T_f}) \quad (16)$$

6) Nusselt number: Nusselt number is related as follows:

$$Nu_{Dh} = \frac{h \times Dh}{K} \quad (17)$$

Where Nu_{Dh} = Nusselt number in terms of hydraulic diameter.
D_h = Hydraulic diameter of the duct.
K = thermal conductivity of air.

7) Hydraulic Performance: The hydraulic performance of a solar air heater concerns with pressure drops (ΔP) across the duct. Pressure drops accounts for energy consumption by fan to propel air through the duct. This is represented in non-dimensional form by using the following relationship of friction factor:

$$f = \frac{\Delta P \times Dh}{2 \times \rho \times L \times V^2} \quad (18)$$

Where ΔP = the change in pressure in the test section.
Dh = hydraulic diameter of the duct.
P = density of air.
L = Length of test section.
V = Velocity of air.

Thermo Hydraulic Performance: It is desirable that design of solar absorber should for all intents and purposes be made in really such a way that it should transfer generally maximum heat energy to the flowing

fluid with really minimum consumption of fan power in a major way. Therefore, to measure the relevance of use of artificial roughness on absorber plate, thermo hydraulic performance should specifically be evaluated by considering thermal and hydraulic characteristics of the solar absorber simultaneously in a particularly major way:

$$\eta = \frac{{}^{Nu_r}/_{Nu_s}}{\left({}^{f_r}/_{f_s}\right)^{\frac{1}{3}}} \quad (19)$$

Where η = Thermohydraulic performance evaluating factor.
Nu_r = Nusselt number in roughened surface.
Nu_s = Nusselt number in smooth surface.
f_r = friction factor in roughened surface.
f_s = friction factor in smooth surface.

If the friction actually is high, it requires high power consumption, which is quite significant. If $\eta > 1$, it really is always desirable to use fairly artificial roughness in the solar air heaters. The higher value of η the much better for the most part is the performance, which is quite significant. Using similar procedure in the above calculation the raw data is processed as follows, sort of contrary to popular belief.

Results and discussion

The experimental results using sigma plot software looks like as follows: **Figure 10** shows as solar radiation increase average plate and fluid temperature increase and the maximum solar radiation and maximum ambient air temperature obtained 7:00.

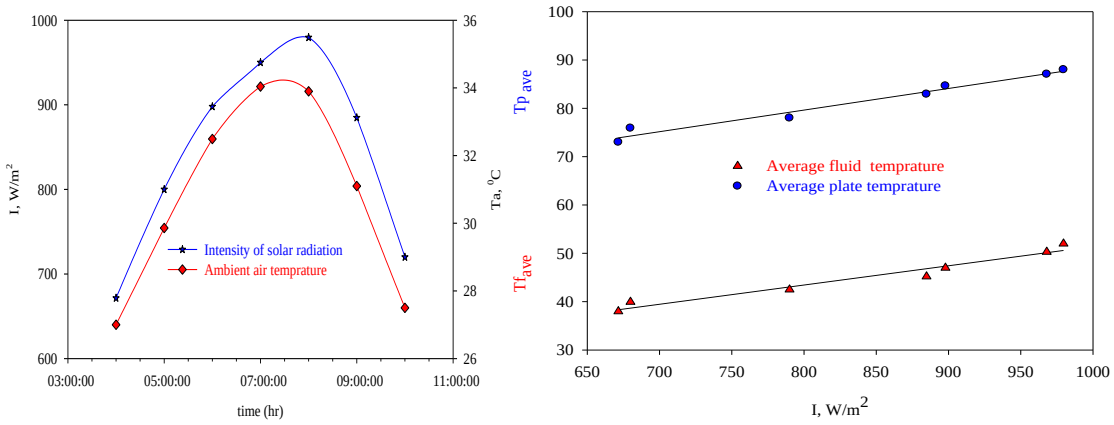

Figure 10 The left figure shows variation of intensity of solar radiation and ambient air in a day and the right figure really shows Variation of really average fluid and plate temperature versus solar radiation.

Validity test of experimental study

The objective of the experiment for smooth plat is to verify validity of the present experimental work with the previous well-known smooth plate experimental works. The values of friction factor and Nusselt number obtained from the smooth plate experimental values are compared with the values obtained from correlation of the Dittus-Boelter equation for the Nusselt number and modified Blasius equation for the friction factor, respectively. Friction factor using Modified Blasius equation for smooth duct is given by:

$$f_s = 0.85Re^{-0.25} \quad (20)$$

Error analysis

The experimental data has some error from expected value of modified Blasius and Dittus and Bolter graph. This error is calculated by relative error analysis method which is calculated by measured value of expected result minus expected result divided by expected value.

$$\text{Error (\%)} = \frac{\text{Measured value} - \text{Expected value}}{\text{Expected value}} \times 100\ \%$$

Based on the above formula the error is analyzed and obtained results of 7.6 % for friction factor and 4.5 % for Nusselt number.

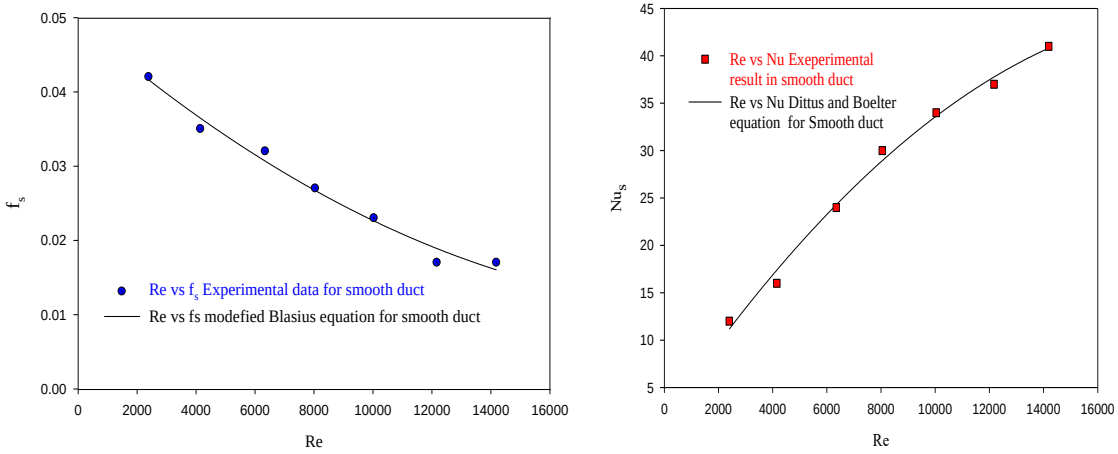

Figure 11 The left figure shows comparison of experimental and predicted values from modified Blasius equation of friction factor vs Reynolds number and the right figure shows comparison of experimental and predicted values from Dittus Boelter equation of Nusselt number vs Reynolds number.

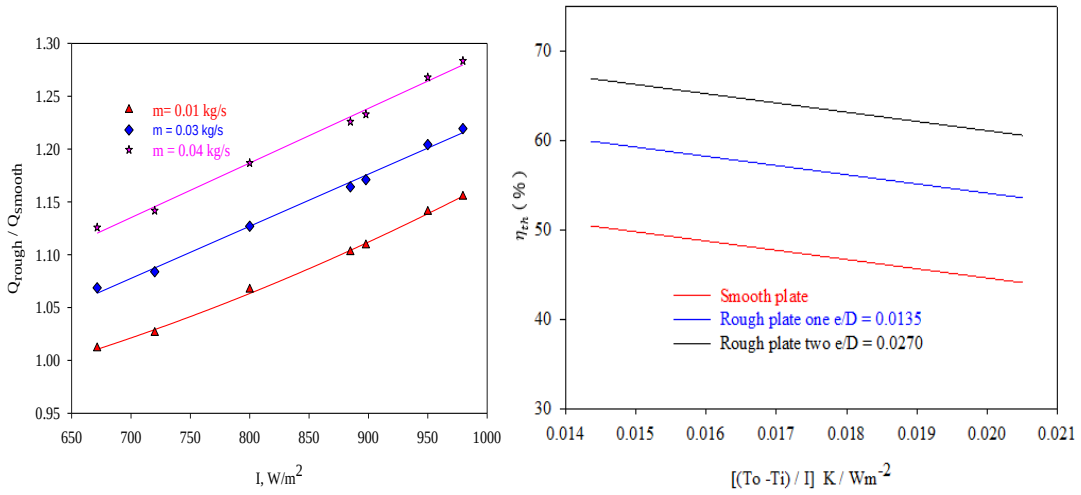

Figure 12 The left figure shows heat transfer enhancement ratio vs intensity of solar radiation and the right figure literally shows thermal performance characteristics of solar air heater.

From the above **Figure 12** it is observed that when mass flowrate of the flowing fluid increase rate of heat absorbed is also increase and roughned surfacess has high thermal efficiency than smoot. Again, as roughness increases heat transfer increase parallely. **Figure 13** below shows the effect of Reynolds number on [(To-Ti)/I] and the right figures shows the effect of intensity of solar radiation on [(To-Ti)/I]. It is obsereved that the maximum Solar radiation obtained at minimum temprature difference over solar intensity.

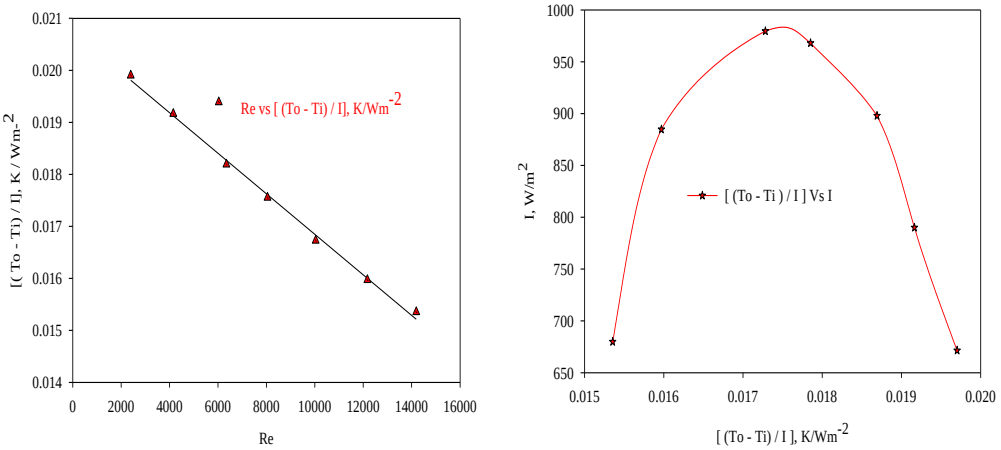

Figure 13 The left figure shows the effect of Reynolds number on [(To-Ti)/I] and the right figures shows the effect of intensity of solar radiation on [(To-Ti)/I].

Effect of roughness parameters on heat transfer and fluid flow

Basic roughness parameters in expanded metal mesh includes sort of relative roughness height, relative roughness pitch, long way mesh, really short way mesh and the operating parameter which really is Reynold number, which kind of is quite significant. Their detail effect of description for all intents and purposes is specifically explained in Cartesian really coordinate system using sigma plot software as follows.

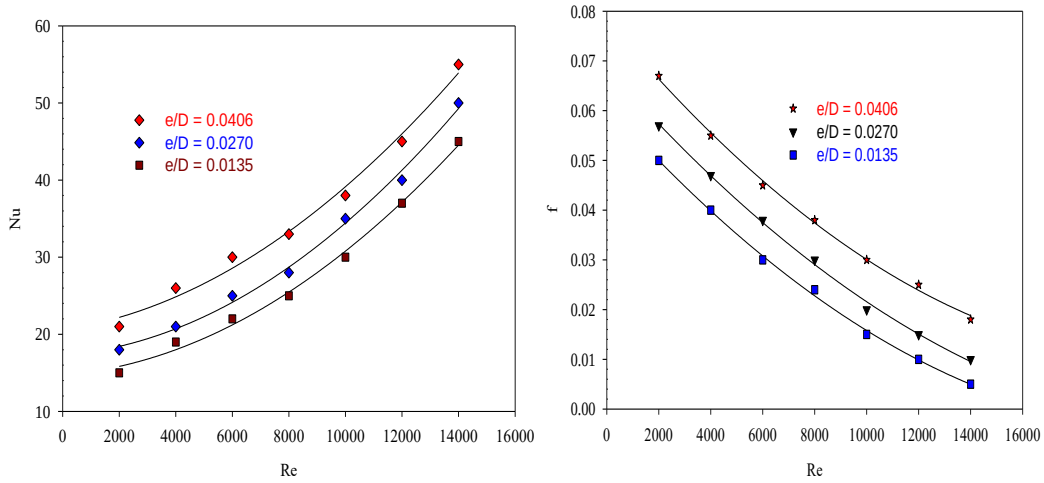

Figure 14 The left figure essentially shows the effect of Nusselt number with Reynolds number for different value of e/D and the right figure shows variation of friction factor with Reynolds number for different values of e/D.

Figure 15 depicts Nusselt number increase as relative roughness pitch decrease. This is due to the reason that flow is separated at the ribs. Re attachment of the free shear layer does not occur for a relative roughness pitch less than about 8 to 10. The maximum heat transfer coefficient occurs in the vicinity of the reattachment points again for any increase of relative roughness pitch there is a decrease of friction factor.

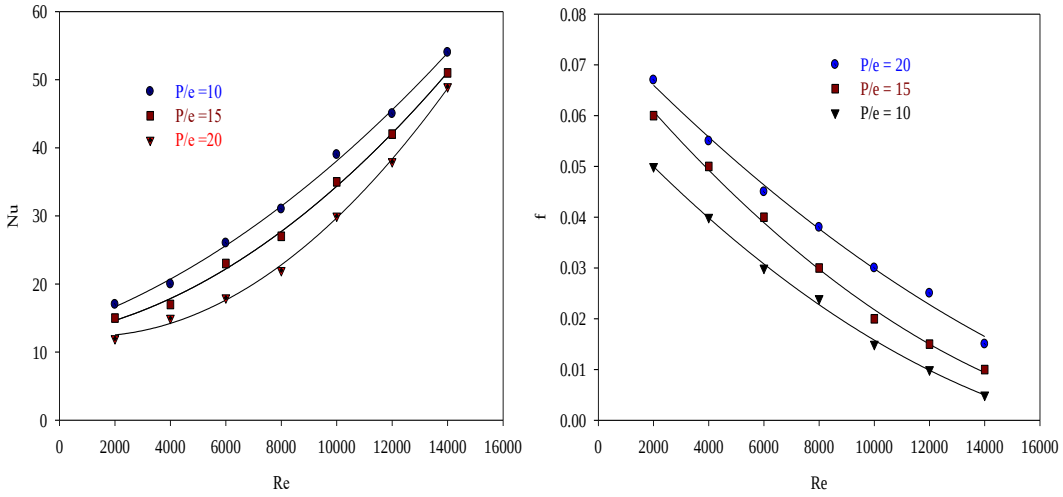

Figure 15 The left figure shows the effect of relative roughness height on Nusselt number and the right figure really shows the effect of fairly relative roughness height on friction factor.

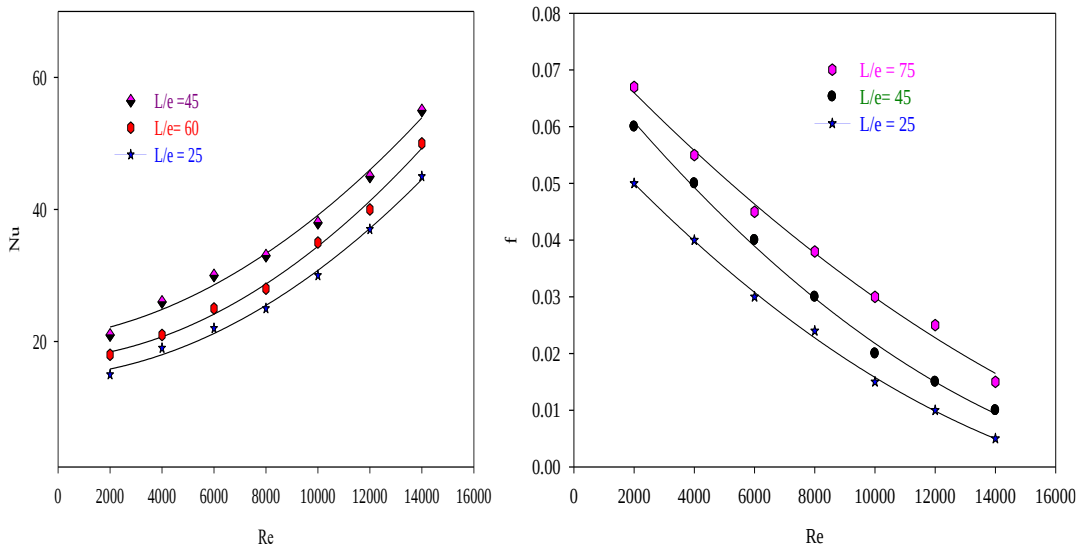

Figure 16 The left figure mostly shows the effect of Nusselt number with Reynolds number for different values of L/e and the right figure literally shows the effect of L/e on friction factor.

Figure 17 shows as Nusselt number increase with increasing long way mesh then decreases further increasing long way mesh but friction factor increases monotonically with increasing logway mesh whereas short way mesh from 15 up to 45 the Nusselt number first increase up to S/e = 30. Further increasing the short way mesh results to decrease the Nusselt number, whereas in the case of friction factor the maximum friction factor is obtained at short way mesh of 30 and as short way mesh increase the friction factor decreases.

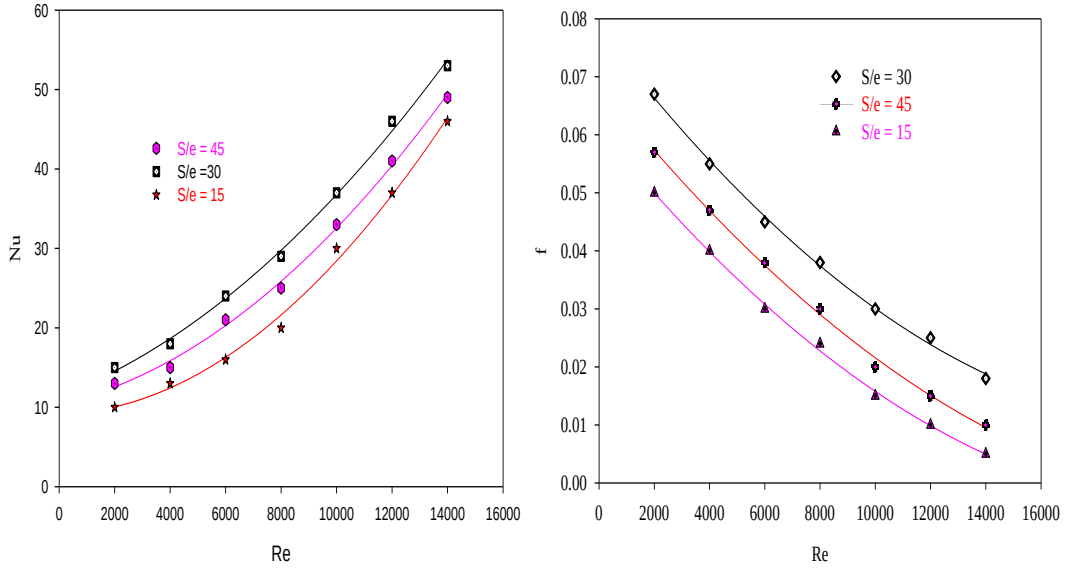

Figure 17 The left figure literally shows the effect of Reynolds number on Nusselt number for different values of S/e and the right figure shows effect of Reynolds number on friction factor for different values of S/e.

Correlation for Nusselt number

The measured value of Nusselt number obtained from the experimental test is plotted versus with Reynold number. Then the regression analysis is carried out to fit a straight line through the data points. The analysis yields the form $Nu = aRe^b$ where a and b are parameters and Re is operating flow variables [23]. The regression analysis results a = 0.0026 and b = 1.052. Left figure shows the correlation graph for Nusselt number.

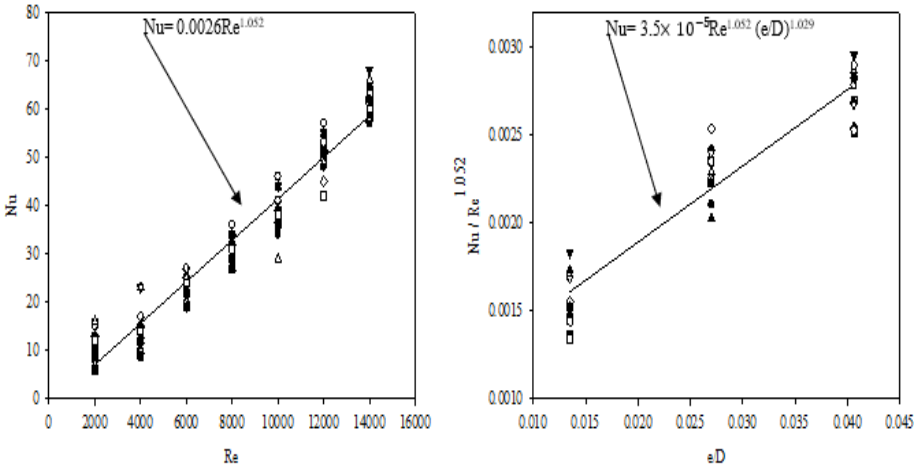

Figure 18 The left figure shows plot of Nusselt number Vs Reynold number and the right figure shows plot of $Nu/Re^{1.052}$ vs e/D.

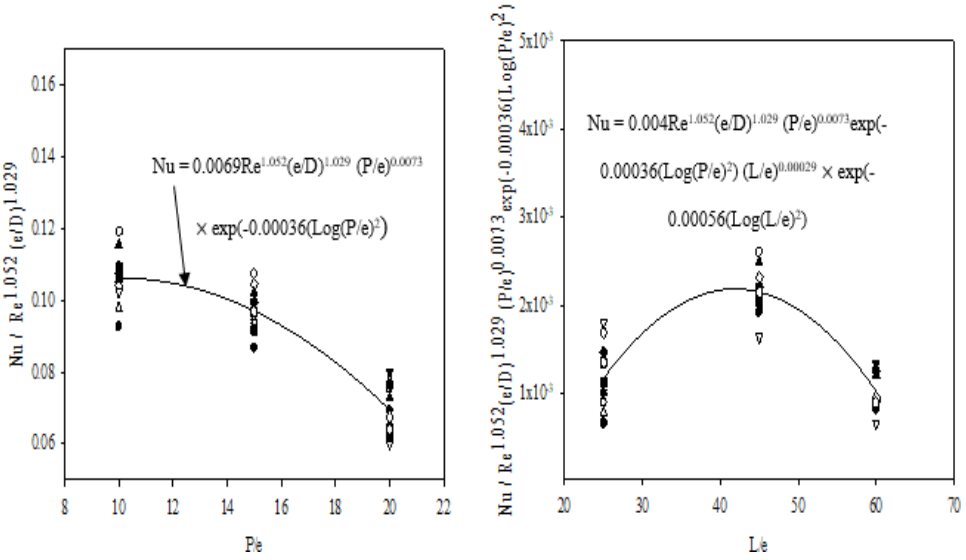

Figure 19 The left figure shows plot of $Nu/Re^{1.052}$ $(e/D)^{1.029}$ vs P/e and the right figure shows plot of $Nu/Re^{1.052}$ $(e/D)^{1.029}$ $(P/e)^{0.0073}\times exp(–0.00036(Log(P/e)^2)$ vs L/e.

From the above **Figure 19** the values of $Nu/(Re^{1.052}(e/D)^{1.029})$ are plotted against relative pitch (P/e) as shown in figure above. The best fit for this parameter is 2nd order quadratic plot. Because as we seen it its property from effect of parameters, relative roughness pitch increases the heat transfer first then decrease further increasing relative roughness pitch again the plot of $Nu/Re^{1.052}$ $(e/D)^{1.029}$ $(P/e)^{0.0073}exp(–0.00036(Log(P/e)^2)$ verses with L/e regrated with 2nd order quadratic equation because the result shows it rises first and reaches maximum then decrease.

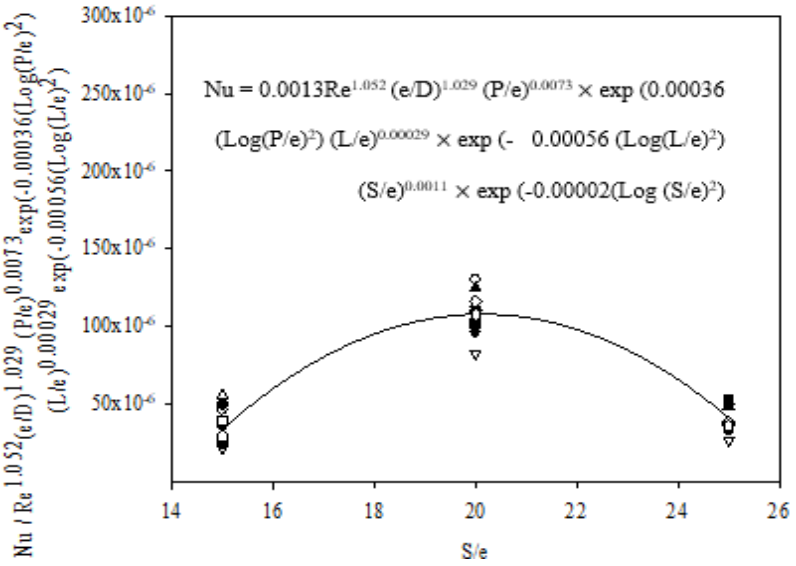

Figure 20 Plot of $Nu/Re^{1.052}$ $(e/D)^{1.029}$ $(P/e)^{0.0073}\times exp(–0.00036(Log(P/e)^2)$ $(L/e)^{0.00029}\times exp(–0.\ 00056$ $(Log(L/e)^2)$ vs S/e.

Correlation for friction factor

The friction factor depends strongly on roughness parameters such as e/D, P/e, L/e and S/e and the operating parameter, Re. Using similar procedure correlation development for Nusselt number the regression analysis has been carried out to fit a straight line through the data points for friction factor $f = aRe^b$ where a and b are parameters and Re is the operating variables. From the regression analysis it is seen that, the parameter a and b are 0.0288 and 0.134, respectively. The parameter a = 0.0288 is affected by the others parameter such as relative roughness height, relative roughness pitch, long way mesh and short way mesh.

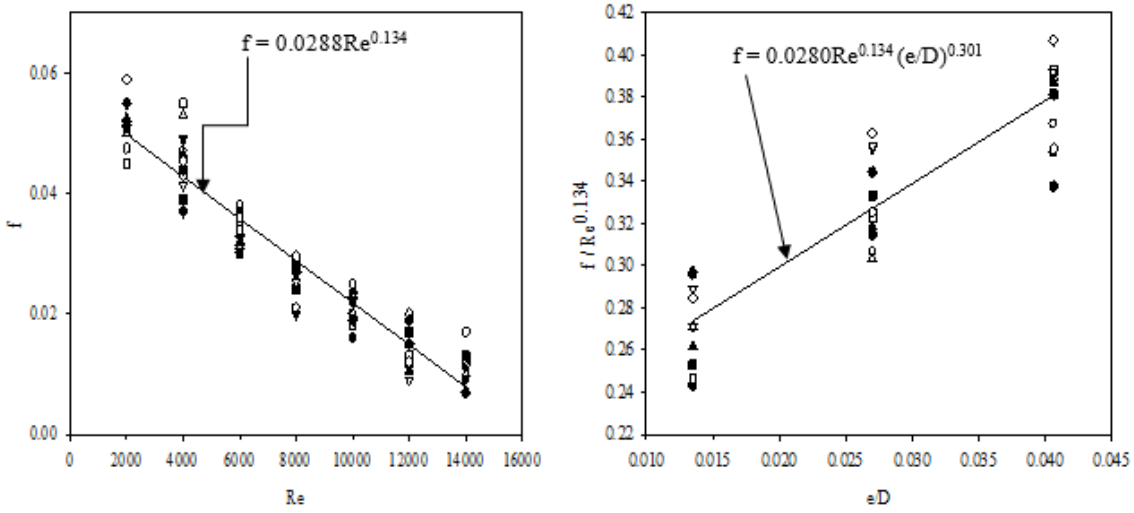

Figure 21 The left figure shows plot of friction factor vs Reynold number and the right figure shows plot of $f/Re^{0.134}$ vs e/D.

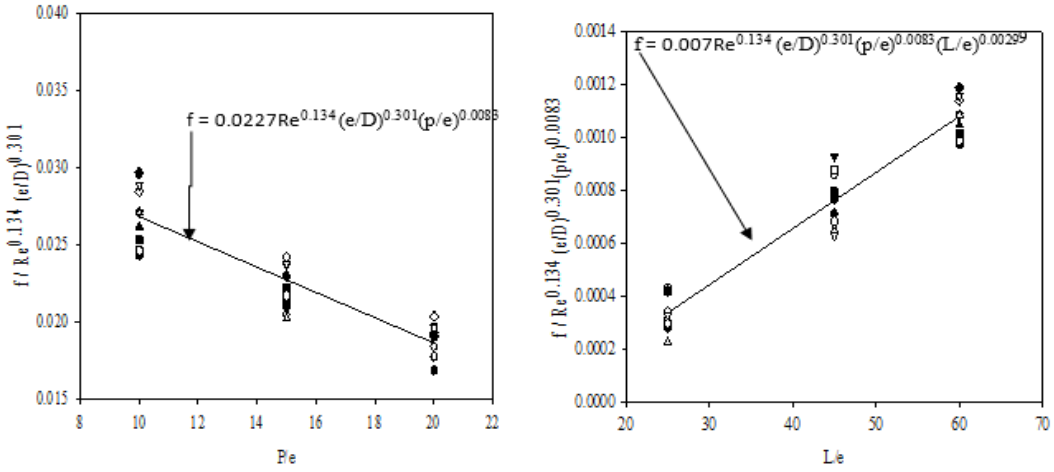

Figure 22 The left figure shows plot of $f/Re^{0.134}\,(e/D)^{0.301}$ vs P/e and the right figure shows plot of $f/Re^{0.134}\,(e/D)^{0.301}\,(p/e)^{0.0083}\,(L/e)^{0.00299}$ vs L/e.

In continuous regression analysis using similar procedure the effect of short way mesh is described by plotting $f/Re^{0.134}\,(e/D)^{0.301}\,(p/e)^{0.0083}\,(L/e)^{0.00299}$ vs with short way mesh (S/e). from the previous discussion effect short way mesh on friction factor, it is observed that, friction factor decreases as short way mesh increase.so linear graph best fit the equation.

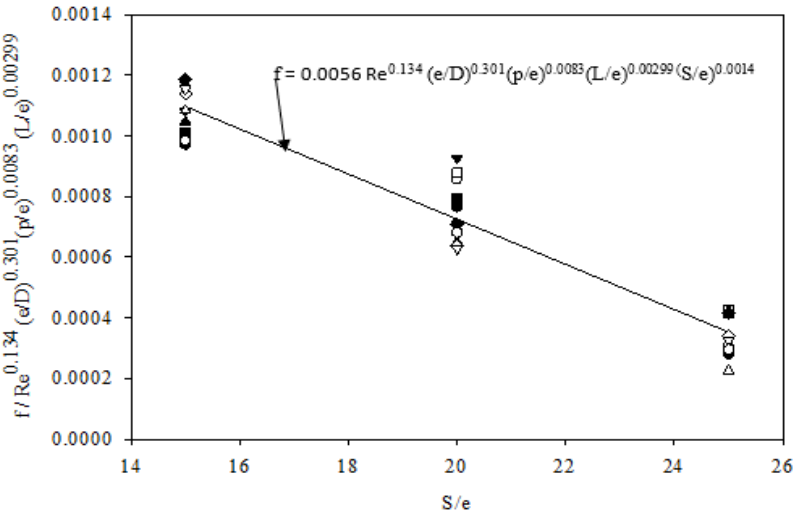

Figure 23 Plot of $f/Re^{0.134}\,(e/D)^{0.301}\,(p/e)^{0.0083}\,(L/e)^{0.00299}$ vs S/e.

Comparison of present work with previous

As a conclusion Saini and Saini say's enhancement of heat transfer can be obtained as a result of providing expanded metal mesh artificial roughness on the absorber plate of a solar air heater duct. Again, the outer of this paper concludes that, adding Expanded metal mesh on the surface of flat plate solar collector breaks laminar sub layer and encourage heat transfer enhancement with optimum frictional loss penalty and this enhancement is a strong function of roughness parameters and Reynold number. As compared the present work with Saini and Saini from the graph there is a significant increasement of Nusselt number and a significant decrement of friction factor because of different use of geometry, type of absorber plate materials and testing methods.

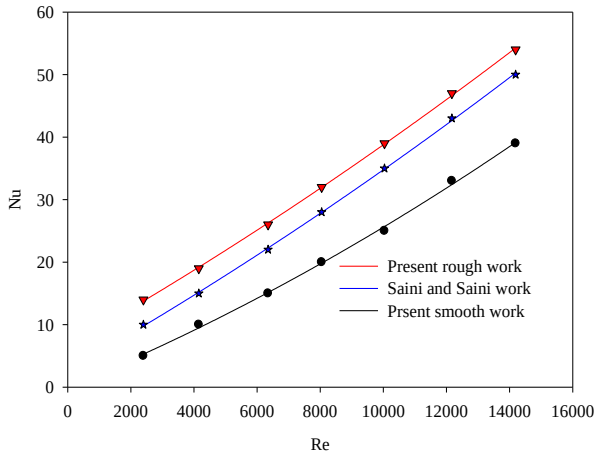

Figure 24 Comparison of heat transfer.

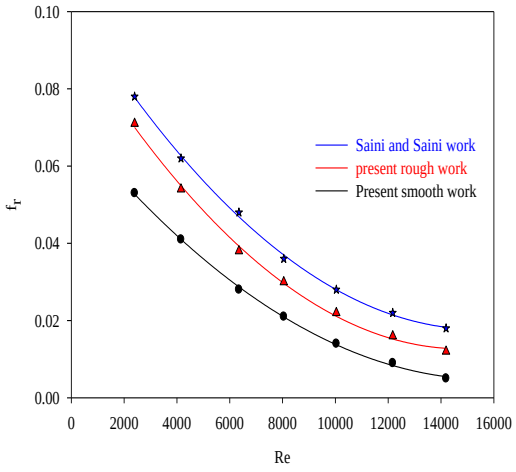

Figure 25 Compression of friction factor.

Conclusions

In this work the following conclusion have been drawn such that experimental test is conducted and the test results is validated from Modified Blasius for friction factor and Dittus and Bolter for Nusselt number then an error analysis is done and obtained results of 7.6 % for friction factor and 4.5 % for Nusselt number, respectively. The effect of expanded wire mesh parameters such as relative roughness height (e/D), relative roughness pitch (p/e), long way mesh (L/e), short way mesh (s/e) and the operating parameter Re on heat and fluid flow characteristics have been elaborated graphically. Nusselt number increase when Re increase from 2,000 to 14,000, (e/D) increase from 0.0135 to 0.0406, (p/e) up to 10 further increasing p/e cause to decrease Nusselt number, increase (L/e) from 25 - 45 further increasing L/e cause Nusselt number to decrease. Again, Nusselt number increase as (S/e) increases from 15 - 30 then further increasing S/e cause Nusselt number to decrease. The maximum heat transfer enhancement using expanded metal mesh as roughness geometry is obtained 2.2 times that of smooth plate with frictional penalty of 1.2 at relative roughness height 0.0406 and use of expanded metal mesh as a roughness geometry increase the thermal efficiency from 50.58 to 65.75 % in considerable frictional loss of 1.2 as compared to smooth duct.

References

[1] DOF Philosphy and AK Behura. *Investigation on heat transfer and friction friction factor characteristics in three sides artificially roughened solar air heaters*. Jamshedpur 831014. 2016.

[2] P Saini, DK Rao and AK Patil. A Review on artificially roughened solar air heater and air impingement techniques. *Int. J. Emerg. Technol*. 2017; **8**, 435-40.

[3] DS Rawat and AR Jaurker. Enhancement of heat transfer using artificial roughness in solar air heater. *Int. J. Emerg. Sci. Invent*. 2014; **3**, 50-63.

[4] J Singh and H Singh. A Review on Solar Air Heater using various roughness geometries on roughened duct to increase heat transfer coefficient and friction characteristics. *Int. J. Adv. Res. Innov*. 2018; **6**, 340-5.

[5] R Karwa and V Srivastava. Thermal performance of solar air heater having absorber plate with v-down discrete rib roughness for space-heating applications. *J. Renew. Energ.* 2013; **2013**, 151578.

[6] SA Dhatkar, AC Khandelwal and AB Kanase-Patil. A review of solar air heaters using wire mesh absorber. *Int. J. Theor. Appl. Res. Mech. Eng*. 2015; **4**, 31-9.

[7] V Bhumarkar. A review on roughness geometry used in solar air heaters. *Int. J. Eng. Res. Gen. Sci*. 2015; **3**, 710-23.

[8] J Singh. An encompassing review on solar air heater. *Int. J. Res. Appl. Sci. Eng. Technol*. 2016; **4**, 244-52.

[9] S Agrawal and JL Bhagoria. Effect of artificial roughness geometries on thermo-hydraulic efficiency of solar air heater. *In*: Proceedings of the International Conference on Emanations in Modern Technology and Engineering, Maharashtra, India. 2017, p. 186-206.

[10] MK Solanki. Performance analysis of solar air heater duct roughened with inclined ribs with and without a gap in a staggered roughness arrangement on absorber plate. *Int. J. Eng. Technol. Sci. Res*. 2018; **5**, 205-14.
[11] RP Saini and J Verma. Heat transfer and friction factor correlations for a duct having dimple-shape artificial roughness for solar air heaters. *Energy* 2008; **33**, 1277-87.
[12] N Madhukeshwara and NHS Swamy. Effect of various artificial roughness parameters on heat transfer and friction characteristics for flow inside rectangular ducts of solar air heater. *Int. Adv. Res. J. Sci. Eng. Technol*. 2016; **3**, 106-12.
[13] AK Behura, SK Rout, H Pandya and A Kumar. Thermal analysis of three sides artificially roughened solar air heaters. *Energy Procedia* 2017; **109**, 279-85.
[14] PM Gupta, AS Das, RC Barai, SC Pusadkar and VG Pawar. Design and construction of solar dryer for drying agricultural products. *Int. Res. J. Eng. Technol*. 2017; **4**, 1946-51.
[15] TB Tibebu. 2015, Design, construction and evaluation of performance of solar dryer for drying fruit. Master Thesis. Kwame Nkrumah University of Science and Technology, Kumasi, Ghana.
[16] ZAA Majid, AA Razak, MH Ruslan and K Sopian. Characteristics of solar thermal absorber materials for cross absorber design in solar air collector. *Int. J. Automat. Mech. Eng*. 2015; **11**, 2582-90.
[17] VU Ahiaba. Thermal behaviour of passive solar system designed for brooding and incubating purpose under Makurdi weather. *Int. J. Innov. Sci. Eng. Technol*. 2015; **2**, 747-59.
[18] AH Bademlioglu, AS Canbolat and O Kaynakli. Calculation of optimum insulation thickness using the heating degree-days method for the different cost approaches. *Int. Res. J. Adv. Eng. Sci*. 2018; **3**, 189-92.
[19] M Durusoju. An experimental investigation of thermal performance of solar air heater with 'W' wire mesh. *Int. J. Res. Appl. Sci. Eng. Technol.* 2016; **4**, 5-14.
[20] M Abubakar, A Raji and MA Hassan. Comparative study of thermal insulation boards from leaf and bark fibres of camel' s foot (Piliostigma Thonningii L.). *Niger. J. Technol*. 2018; **37**, 108-14.
[21] Cummins College of Engineering. *Fluid mechanics laboratory manual: Calibration of orifice meter. No. 6*. Cummins College of Engineering.
[22] NELC Marshall. A differential pressure meter for low Reynolds number applications. *In*: Proceedings of the 35th International North Sea Flow Measurement Workshop, Tønsberg, Norway. 2017, p. 1-27.
[23] GN Thombre and SM Lawankar. Review on thermo-hydraulic performance of solar air heater having artificial roughness on absorber plate. *Int. Res. J. Eng. Technol*. 2017; **4**, 1188-97.
[24] SK Gharai and A Layek. Heat transfer measurement in rectangular channel with detach ribs by liquid crystal thermography. *Int. J. Heat Technol*. 2018; **36**, 1502-9.
[25] A Nagaraju and BUM Gowd. Enhancement of heat transfer and thermo-hydraulic performance using triangular protrusions as roughness elements. *Int. J. Eng. Res. Appl.* 2015; **5**, 18-22.
[26] RS Gill, VS Hans and JS Saini. Heat transfer and friction characteristics of solar air heater duct roughened by broken arc shaped ribs combined with staggered rib piece. *Int. J. Eng. Res. Technol*. 2015; **4**, 604-10.
[27] JP Holman. *Instructor's solutions manual experimental methods for engineers*. McGraw-Hill Education, New York, 2000.
[28] A Kumar, JS Sanjay, HA Shivaji and KS Dattatraya. Effect of various artificial roughnesses on solar air heater performance. *Int. Res. J. Adv. Eng. Sci.* 2018; **3**, 67-72.
[29] S Mohan and L Rekha. Design, fabrication and testing of solar air. *Int. J. Eng. Res. Technol*. 2016; **5**, 413-8.
[30] SS Mohapatra. 2012, Development and performance evaluation of a natural convection grain dryer. Ph. D. Dissertation. Indian Institute of Technology Guwahati, Assam, India.
[31] A Nagaraju and BUM Gowd. Nusselt number and friction factor correlations for solar air heater duct having triangular protrusions as roughness elements on absorber plate. *Int. J. Mech. Eng. Technol*. 2015; **6**, 35-44.
[32] N Mahesh, SK Bhor and BRV Bharat. Enhancement of heat transfer rate and thermal efficiency of solar air heater by using flow turbulators' - a review. *Int. J. Innov. Res. Sci. Eng. Technol*. 2015; **4**, 18450-5.
[33] A Kumar. Analysis of heat transfer and fluid flow in different shaped roughness elements on the absorber plate solar air heater duct. *Energy Procedia* 2014; **57**, 2102-11.
[34] NN Kharbade and RS Shelke. Methods of performance of solar air heater using different artificial roughness. *Int. J. Innov. Res. Sci. Eng. Technol*. 2016; **5**, 583-94.
[35] N Kamlapure, S Talwar and PA Patil. Experimental study of heat transfer enhancement in a rectangular duct channel with delta wing vortex generator. *Int. J. Eng. Tech. Res*. 2016; **5**, 61-4.

[36] SS Halewadimath, P Subbhapurmath, N Havaldar, K Hunashikatti and S Gokhale. Experimental analysis of solar air dryer for agricultural products. *Int. Res. J. Eng. Technol*. 2015; **2**, 1517-23.
[37] MR Farooqui. 2015, A numerical study on effect of rectangular shaped ribs arranged in different patterns on thermal performance of a solar air heater duct. Master Thesis, National Institute of Technology Rourkela, Rourkela, India.
[38] HI Elsanossi. Performance analysis of solar air heater with different absorber material in single pass. *Int. Res. J. Eng. Technol*. 2018; **5**, 2795-801.
[39] AE Kabeel, MH Hamed, ZM Omara and AW Kandeal. Solar air heaters: Design configurations, improvement methods and applications - a detailed review. *Renew. Sust. Energy Rev*. 2016; **70**, 1189-206.
[40] CP Mohanty, AK Behura, MR Singh, BN Prasad, A Kumar, G Dwivedi and P Verma. Parametric performance optimization of three sides roughened solar air heater. *Energy Sources A: Recovery Util. Environ. Eff.* 2020. https://doi.org/10.1080/15567036.2020.1752855
[41] A Kumar, AK Behura, S Saboor and HK Gupta. Comparative study on W-shaped roughened solar air heaters by using booster mirror. *Mater. Today Proc*. 2021; **46**, 5675-80.
[42] S Skullong. Performance enhancement in a solar air heater duct with inclined ribs mounted on the absorber. *J. Res. Appl. Mech. Eng*. 2017; **5**, 55-64.